First-principles study of the dielectric and dynamical properties of orthorhombic $CaMnO_3$

2008 J. Phys.: Condens. Matter 20 255229

(http://iopscience.iop.org/0953-8984/20/25/255229)

J. Phys.: Condens. Matter **20** (2008) 255229 (5pp) doi:10.1088/0953-8984/20/25/255229

First-principles study of the dielectric and dynamical properties of orthorhombic $CaMnO_3$

Satadeep Bhattacharjee, Eric Bousquet and Philippe Ghosez

Physique Théorique des Matériaux, Université de Liège Allée du 6 Août 17, B-4000 Sart Tilman, Belgium

Received 10 March 2008, in final form 30 April 2008
Published 22 May 2008
Online at stacks.iop.org/JPhysCM/20/255229

Abstract

The structural, dielectric and dynamical properties of the low temperature antiferromagnetic orthorhombic phase of $CaMnO_3$ have been computed from first principles, using a density functional theory approach within the local spin density approximation. The theoretical structural parameters are in good agreement with experiment. The full set of zone-center phonons is reported, allowing new assignment of experimental Raman data and providing reference values for the interpretation of future infrared phonon measurements. It is shown that the static dielectric constant is very large and comparable in amplitude to that of isostructural $CaTiO_3$. In contrast to the pseudocubic structure, it is also highly anisotropic. These features are discussed in relationship to the anomalous Born effective charges and the presence of low frequency polar modes.

1. Introduction

Magnetic perovskite oxides constitute an exciting subject of study. Indeed, the interplay between their structural, magnetic and transport properties make them fascinating from both experimental and theoretical points of view. For example, the mixed valency perovskite $Ca_{1-x}La_xMnO_3$ is one of the most studied materials for its colossal magnetoresistance [1]. Also, the oxygen deficient manganites $LaMnO_{3-\delta}$ and $CaMnO_{3-\delta}$ are interesting for their transport and optical properties [2].

In this paper we report a first-principles study of stoichiometric $CaMnO_3$. The ground-state crystal structure of $CaMnO_3$ is orthorhombic with space group *Pnma* [4]. The structure can be regarded as a distorted perovskite structure having four formula units [4, 5]. It is an insulator with an observed bandgap of about 3 eV [6]. The formal ionic configuration of $CaMnO_3$ is Ca^{2+} Mn^{4+} O^{2-}. In the octahedral crystal field, the 5d orbitals of the Mn^{4+} ion split into lower three-fold degenerated t_{2g} levels and higher two-fold degenerated e_g levels; the occupation being t_{2g}^3 and e_g^0 [7]. Because of the Mn^{4+} configuration, there is no tendency to Jahn–Teller distortion. The magnetic structure is antiferromagnetic and the G-type order is energetically the most favorable. The magnetic interactions between the Mn ions are due to superexchange interactions. The observed Néel temperature is about 130 K [8], which estimates the exchange energy to be around 6.6 meV.

Previous first-principles calculations on $CaMnO_3$ focused mainly on the cubic phase and the electronic structure of the system. Here, we report a first-principles study of the dielectric and dynamical properties of the ground-state orthorhombic phase. This will allow us to reinvestigate the previous assignment of experimental Raman data and to provide benchmark results for the infrared active modes. It will also point out that the static dielectric constant is not only surprisingly large, and comparable to that of isostructural $CaTiO_3$, but also highly anisotropic, which is unexpected in view of the pseudocubic character of the structure.

2. Technical details

The first-principles simulations were performed according to the density functional theory scheme (DFT) within the local spin density approximation (LDA) and using the plane-wave implementation of the ABINIT package [9]. We used the Hartwigsen–Goedecker–Hutter (HGH) [10] parametrization for the pseudopotentials, where the 3s and 3p orbitals were treated as valence states for Mn and Ca atoms and 2s and 2p orbitals were considered as valence states for O atoms. The total number of valence states is therefore 15 for Mn, 10

for Ca and 6 for oxygen. Convergency was reached for an energy cutoff of 72 Hartree for the plane-wave expansion and a $6 \times 4 \times 6$ k-point mesh for the Brillouin zone integration. The phonon frequencies, Born effective charges and dielectric tensor were computed according to the density functional perturbation theory (DFPT) [11] scheme as implemented in the ABINIT package.

3. Structural properties

At high temperature, $CaMnO_3$ adopts a cubic perovskite structure. At room temperature it exhibits an orthorhombic *Pnma* (N.62) structure [12] with 20 atoms in the primitive unit cell, which moreover exhibits a G-type antiferromagnetic order below 130 K [4]. This orthorhombic phase results from the condensation into the cubic structure of three antiferrodistortive (AFD) instabilities which are related to tilts of oxygen octahedra around the Mn–O axis. In Glazer's notation, these tilts are described by $a^-b^+c^-$. Since these oxygen rotations do not strongly affect the highly symmetric structure, the orthorhombic phase of $CaMnO_3$ can be described as a pseudocubic structure, the volume of which can be estimated as $\sqrt{2}a_c \times 2a_c \times \sqrt{2}a_c$ where a_c is the pseudocubic cell parameter.

In our calculations, we imposed a G-type antiferromagnetic order and did the structural relaxation at fixed volume. The chosen volume is associated to a pseudocubic cell parameter of 3.73 Å which corresponds to the experimental cubic lattice constant [3] and also closely agrees with the experimental pseudocubic lattice constant of the orthorhombic phase [4]. The cell shape and atomic positions were relaxed according to this constraint and the results are reported in table 1.

The relaxed structure is in excellent agreement with the experimental data. The cell parameters a and b are only slightly overestimated while the c parameter is slightly underestimated (errors of ≈0.5%). The calculated atomic positions are also in good agreement with the experimental data, the distortion with respect to the ideal cubic positions being predicted with an accuracy similar to what is usually achieved in the class of ABO_3 compounds [13].

From the inspection of the density of states, we found a theoretical electronic bandgap of 0.8 eV for our relaxed antiferromagnetic orthorhombic structure. Although this strongly underestimates the experimental value (3.1 eV [14]), as usual within the LDA, our calculation properly reproduces the insulating character of the structure.

4. Dielectric properties

The Born effective charge of a given atom κ is a dynamical concept that is related to the change of polarization induced by an atomic displacement [17]. It is a tensor that is formally defined as:

$$Z^*_{\kappa,\alpha\beta} = \Omega_0 \frac{\partial P_\beta}{\partial \tau_{\kappa,\alpha}}\bigg|_{E=0} \quad (1)$$

where Ω_0 is the unit-cell volume and the derivative is evaluated under the condition of vanishing macroscopic electric field.

Table 1. Theoretical and experimental unit-cell parameters (Å) and non-equivalent atomic positions (reduced coordinates) in the antiferromagnetic orthorhombic *Pnma* structure of $CaMnO_3$. The Wyckoff positions of the reported atoms are mentioned in brackets.

	Orthorhombic		Pseudocubic
	This work	Exp. [4]	Exp. [15]
a	5.287	5.279	5.275
b	7.498	7.448	7.460
c	5.235	5.264	5.275
a_c	3.730	3.726	3.730
Ca (4c)			
x	0.040	0.033	0.000
y	0.250	0.250	0.250
z	−0.008	−0.006	0.000
Mn (4b)			
x	0.000	0.000	0.000
y	0.000	0.000	0.000
z	0.500	0.500	0.500
O_1 (4c)			
x	0.485	0.490	0.500
y	0.250	0.250	0.250
z	0.071	0.066	0.000
O_2 (8d)			
x	0.287	0.287	0.250
y	0.036	0.034	0.000
z	−0.288	−0.288	0.250

The Born effective charges have been calculated for the four atoms of table 1. The full tensors are as follows:

$$Z^*(\mathrm{Ca}) = \begin{pmatrix} 2.51 & 0.00 & 0.19 \\ 0.00 & 2.43 & 0.00 \\ 0.27 & 0.00 & 2.52 \end{pmatrix} \quad [2.29 \quad 2.74 \quad 2.43]$$

$$Z^*(\mathrm{Mn}) = \begin{pmatrix} 6.82 & -0.37 & -0.72 \\ 0.07 & 5.78 & 1.42 \\ -0.69 & -1.54 & 6.56 \end{pmatrix} \quad [7.41 \quad 6.05 \quad 5.70]$$

$$Z^*(\mathrm{O_1}) = \begin{pmatrix} -1.73 & 0.00 & 0.06 \\ 0.00 & -5.11 & 0.00 \\ -0.20 & 0.00 & -1.76 \end{pmatrix} \quad [-1.67 \quad -1.82 \quad -5.11]$$

$$Z^*(\mathrm{O_2}) = \begin{pmatrix} -3.80 & -0.08 & -1.94 \\ -0.11 & -1.55 & -0.01 \\ -1.97 & 0.00 & -3.61 \end{pmatrix} \quad [-5.66 \quad -1.77 \quad -1.53].$$

Below each tensor, the main values of the symmetric part of Z^* are also mentioned, for direct comparison with (i) the nominal atomic charges ($Z_N(\mathrm{Ca}) = +2$, $Z_N(\mathrm{Mn}) = +4$ and $Z_N(\mathrm{O}) = -2$) and (ii) the Born effective charges in the cubic phase at $a_c = 3.73$ Å ($Z^*_C(\mathrm{Ca}) = +2.61$, $Z^*_C(\mathrm{Mn}) = +7.43$, $Z^*_C(\mathrm{O}_\perp) = -2.55$ and $Z^*_C(\mathrm{O}_\parallel) = -4.94$). First, we notice the *anomalously* large values of the Mn and O charges, which are significantly larger than the nominal atomic charges. These values are rather similar to those previously reported for the isostructural $CaTiO_3$ [16] and also to those in most ferroelectric and related ABO_3 compounds [13, 17]. In the latter, the anomalously large $Z^*(\mathrm{O})$ and $Z^*(\mathrm{B})$ were related to the partial hybridization between O 2p and B-metal d

states [17]. It is therefore slightly surprising to get comparable values in $CaMnO_3$ and $CaTiO_3$ for which the nominal d-state occupation is different. However, the amplitude of Z^* is not sensitive to the *amplitude* of the hybridizations but to the *dynamical changes* of these hybridizations under atomic displacement. The present result teaches us that hybridizations in $CaMnO_3$ are similarly sensitive to atomic distortion as they are in the titanates. As usual also in the family of ABO_3 compounds, there is a reduction of the anomalous values in the low symmetry phase in comparison to those in the highly symmetric cubic structure, with the exception here of $Z^*_{yy}(O_1)$. Finally, we notice the existence of small asymmetric contributions, as allowed by symmetry in the orthorhombic phase. Although its value is not expected to be fully accurately predicted within the LDA [18], we also report the calculated optical dielectric tensor:

$$\epsilon_\infty = \begin{pmatrix} 11.3 & 0.0 & 0.0 \\ 0.0 & 13.1 & 0.0 \\ 0.0 & 0.0 & 10.8 \end{pmatrix}.$$

The calculated tensor is only slightly anisotropic, coherently with the pseudocubic character of the structure. Its elements are significantly larger than in related compounds like $CaTiO_3$ ($\epsilon_\infty \approx 6$ [16]), as expected from the smaller LDA bandgap of $CaMnO_3$. The optical dielectric tensor in the orthorhombic phase does not differ significantly from that previously reported in the ideal cubic structure ($\epsilon_\infty = 10.43$ from our calculations and $\epsilon_\infty = 11.25$ from [19]). We notice, however, that it is slightly larger than in the cubic phase, which is a trend different from that reported for orthorhombic $CaTiO_3$ in which ε_∞ decreases when non-polar distortions are frozen into the structure [16].

5. Dynamical properties

The irreducible representation in the orthorhombic *Pnma* phase $CaMnO_3$ at the Γ point is:

$$7A_g \oplus 5B_{1g} \oplus 7B_{2g} \oplus 5B_{3g} \oplus 10B_{1u} \oplus 8B_{2u} \oplus 10B_{3u} \oplus 8A_u.$$

Over this decomposition, three modes are acoustic (symmetries B_{1u}, B_{2u}, B_{3u}), eight are silent (symmetry A_u), 24 are Raman (R) active (symmetries A_g, B_{1g}, B_{2g} and B_{3g}) and the last 25 modes are infrared (IR) active (symmetries B_{1u}, B_{2u} and B_{3u}). According to the structure defined in table 1, the IR B_{3u} modes are polarized along the x direction, B_{2u} along the y direction and B_{1u} along the z direction. The eight A_u silent modes, not further discussed below, are calculated at frequencies of 123, 140, 179, 220, 313, 392, 438 and 466 cm^{-1}.

5.1. Raman active modes

We report in table 2 the calculated frequencies of the Raman active modes and a related new assignment of the experimental data. The latter are compared to the assignment previously proposed from shell-model results in [15].

Experimentally, the main observed modes are those of A_g symmetry. ten A_g modes were measured at 150, 160, 184, 243, 278, 322, 382, 438, 487 and 615 cm^{-1} while only seven modes are expected from group theory. The frequency at 615 cm^{-1} was unambiguously assigned to impurity and the modes at 382 and 438 cm^{-1} were kept aside since their frequencies differ strongly from those of the shell model. Below 200 cm^{-1} the assignment was particularly ambiguous since two modes were calculated at 154 and 200 cm^{-1}, while three were observed in the spectra.

Table 2. Comparison of the calculated and experimental frequencies (cm^{-1}) of the Raman modes of the antiferromagnetic orthorhombic phase of $CaMnO_3$. The first column labels the symmetry of each mode. The second and third columns correspond to the present first-principles (FP) calculations and the related assignment of the experimental data of [15]. The fourth and fifth columns correspond to the shell-model (SM) calculations and related assignment in [15].

	Present		Reference [15]	
Symmetry	FP	Exp. [15]	SM	Exp.
A_g	152	150	154	160
A_g	167	160	200	184
B_{2g}	172	—	148	—
B_{2g}	180	—	232	258
B_{1g}	189	179	178	179
B_{3g}	203	—	290	—
B_{2g}	227	258	292	—
B_{1g}	241	—	281	—
A_g	250	243	242	243
A_g	275	278	299	278
A_g	314	322	345	322
B_{3g}	320	320	304	320
B_{1g}	330	—	354	—
B_{2g}	372	—	366	—
B_{2g}	425	—	453	465
B_{3g}	434	—	459	—
A_g	450	438	467	487
B_{2g}	465	465	485	—
B_{3g}	469	—	541	564
B_{1g}	488	—	536	—
A_g	504	487	555	—
B_{1g}	595	564	743	—
B_{2g}	655	—	749	—
B_{3g}	674	—	754	—

From our calculation, the experimental lines at 243, 278 and 322 cm^{-1} can be assigned to the A_g modes at 250, 275 and 314 cm^{-1} respectively. For the low frequencies, the assignment can be significantly improved if we assign to the calculated modes at 152 and 167 cm^{-1}, the experimental modes at 150 and 160 cm^{-1} rather than those at 160 and 184 cm^{-1} as previously proposed (i.e. ruling out the experimental mode at 184 cm^{-1} instead of the one at 150 cm^{-1}). For the high frequency A_g modes, the overall agreement between experimental and theoretical data is best if we assign the experimental line at 438 cm^{-1} (not assigned in [15]) to the calculated mode at 450 cm^{-1} and the one at 487 cm^{-1} to the calculated mode at 504 cm^{-1}.

The experimental line at 179 cm^{-1}, assigned to a B_{1g} mode in [15], is in good agreement with our calculation (189 cm^{-1}). Amongst the two experimental lines at 320 and 564 cm^{-1} previously assigned to B_{3g} modes [15], only the first one is reproduced within our calculation with a very good accuracy (320 cm^{-1}) while, for the second one, we get a theoretical frequency of 469 cm^{-1}. Since the assignment between B_{1g} and B_{3g} modes is rather ambiguous, we propose that the

Table 3. Symmetry and frequency of the 25 IR modes. The mode effective charges ($\overline{Z}^*_{m,\alpha\alpha}$, as defined in [11]) and the oscillator strengths ($S_m^{\alpha\alpha}$) are also provided for each mode as well as the contribution to the static dielectric constant $\varepsilon_{0,m}^{\alpha\alpha}$. From our conventions, $\alpha\alpha = xx$ for B_{3u} modes, $\alpha\alpha = yy$ for B_{2u} modes and $\alpha\alpha = zz$ for B_{1u} modes.

Symmetry	ω (cm^{-1})	$\overline{Z}^*_{m,\alpha\alpha}$ ($\lvert e^-\rvert$)	$S_m^{\alpha\alpha}$ (10^{-4} a.u.)	$\varepsilon_{0,m}^{\alpha\alpha}$ (–)
B_{3u}	101	15.95	57.0	238.40
B_{1u}	147	10.74	17.00	35.09
B_{1u}	150	13.63	34.00	65.37
B_{3u}	153	3.97	2.20	4.06
B_{2u}	155	2.03	0.43	0.70
B_{2u}	179	5.60	8.50	11.40
B_{2u}	208	14.26	38.00	37.67
B_{1u}	215	5.60	6.30	5.80
B_{3u}	216	3.10	1.70	1.50
B_{3u}	234	5.06	5.00	3.90
B_{2u}	251	4.60	5.60	3.80
B_{3u}	287	3.40	3.50	1.80
B_{1u}	290	0.59	0.09	0.04
B_{2u}	324	2.70	0.98	0.37
B_{1u}	326	2.59	1.90	0.78
B_{3u}	340	1.40	0.36	0.13
B_{1u}	345	2.36	1.40	0.51
B_{1u}	381	6.18	6.10	1.80
B_{1u}	414	0.06	0.00	0.00
B_{3u}	423	1.92	1.20	0.25
B_{2u}	437	1.89	1.20	0.26
B_{3u}	469	4.22	5.50	1.07
B_{2u}	488	4.14	5.70	1.04
B_{3u}	495	1.40	0.54	0.09
B_{1u}	504	3.40	3.80	0.65

experimental line at 564 cm^{-1} might in fact correspond to the B_{1g} mode calculated at 595 cm^{-1}.

Finally, from [15], it seems that the B_{2g} modes are theoretically predicted with less accuracy since modes calculated with the shell model at 180 and 425 cm^{-1} are associated to the lines measured at 258 and 465 cm^{-1}. From our first-principles calculation, this agreement seems significantly better and we propose to assign the experimental line at 258 cm^{-1} to the theoretical mode at 227 cm^{-1} and the line at 465 cm^{-1} to the theoretical mode at 465 cm^{-1}.

It can be mentioned here that Perebeinos and Allen [20] predicted resonant behavior of Raman scattering in $LaMnO_3$ with the orbital excitation energy close to the Jahn–Teller gap. Such effects are, however, unexpected here since in this case e_g orbitals are not Jahn–Teller unstable and remain degenerated.

5.2. IR active modes

Table 3 summarizes the calculated IR frequencies of the TO modes, while in figure 1 we report the calculated IR reflectivity spectra (without damping) at normal incidence, respectively on the [100], [010] and [001] surface of a $CaMnO_3$ monocrystal for direct comparison with experimental data. Unfortunately no IR measurement on monocrystal in the orthorhombic phase of $CaMnO_3$ was found to compare with our results. An IR spectra was reported in [21] but on a polycrystalline sample, and no symmetry attribution was reported for the 15

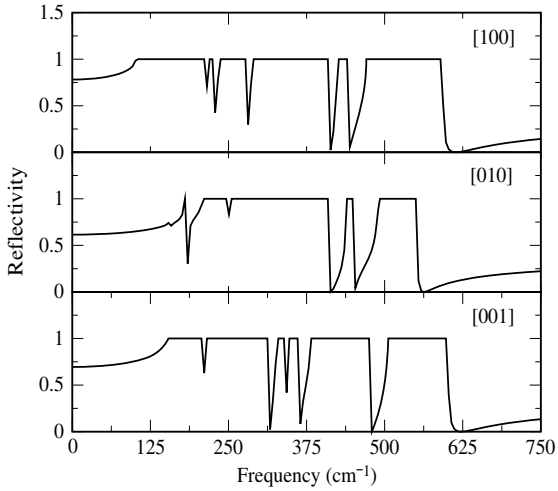

Figure 1. Calculated IR reflectivity spectra (without damping) at normal incidence on the [100], [010] and [001] surface of a $CaMnO_3$ monocrystal in the orthorhombic phase.

observed frequencies, which makes comparison very difficult considering the high number of modes. The only remark that can be made concerns the high frequency part of the spectrum. The three highest frequencies are measured in [21] at 533, 580 and 628 cm^{-1}, which deviate strongly with our results where the maximum frequency of IR modes is calculated at 504 cm^{-1}. This could eventually be related to inaccuracies in our calculations but also suggests that these experimental frequencies might correspond to a combination of modes (for example, the highest measured frequency 628 cm^{-1} can be recovered as being the exact sum of the modes calculated at 305 and 323 cm^{-1}).

In addition to the frequencies, we also report in table 3 the mode effective charges [11], the oscillator strengths and the contribution of each polar mode to the static dielectric tensor. The total static dielectric tensor can be decomposed as follows:

$$\epsilon_0^{\alpha\beta} = \epsilon_\infty^{\alpha\beta} + \sum_m \epsilon_{0,m}^{\alpha\beta} \tag{2}$$

where α and β are the Cartesian directions (x, y or z), ϵ_∞ is the optical dielectric tensor and $\epsilon_{0,m}$ is the contribution to the dielectric constant of each individual phonon mode m. This latter contribution is computed from the following relation:

$$\epsilon_{0,m}^{\alpha\beta} = \frac{4\pi}{\Omega}\frac{S_m^{\alpha\beta}}{\omega_m^2} \tag{3}$$

where Ω is the volume of the cell, $S_m^{\alpha\beta}$ and ω_m are respectively the oscillator strength and the frequency of the mode m.

The computed static dielectric tensor is reported below:

$$\epsilon_0 = \begin{pmatrix} 262 & 0.0 & 0.0 \\ 0.0 & 68 & 0.0 \\ 0.0 & 0.0 & 120 \end{pmatrix}.$$

This also corresponds to an average dielectric constant, $\epsilon_0^{\text{av}} = \frac{1}{3}(\epsilon_0^{xx} + \epsilon_0^{yy} + \epsilon_0^{zz}) = 150$ which is the quantity that one would measure in an ideal ceramic sample with randomly oriented grains.

First we notice that the dielectric constant of $CaMnO_3$ is particularly large, especially along the x direction, and takes values comparable to those previously reported for the orthorhombic phase of $CaTiO_3$ [16]. In the latter case, the large dielectric constant was associated with the 'incipient ferroelectric' character of the compound. The present result suggests that the same type of behavior might be true in $CaMnO_3$. Second, the static dielectric tensor does not only take very large values but is also highly anisotropic. This strongly contrasts with what was reported for the optical dielectric tensor and is also unexpected in view of the pseudocubic character of the structure.

Some insight into these results is provided from equation (3) and inspection of table 3. Along the x direction, the large static dielectric constant ($\epsilon_0^{xx} = 262$) originates essentially in the contribution of the lowest B_{3u} mode at 101 cm^{-1} (238), which combines giant mode effective charge and oscillator strength and a low frequency. Along the z direction, there are still highly polar modes (B_{1u}) with giant mode effective charge but at higher frequencies so that the static dielectric constant is smaller. Along the y direction, the most polar mode (B_{2u}) is at a still larger frequency. So, although, the distortion from the cubic phase is small and the material remains optically rather isotropic, the small distortions are enough to produce strong anisotropy of the dynamical properties.

6. Conclusion

The structural, dielectric and dynamical properties of the antiferromagnetic orthorhombic phase of $CaMnO_3$ have been studied from first principles. The relaxed structure is in good agreement with experimental data. As within the cubic phase, the Born effective charges of Mn and O are highly anomalous. The whole set of zone-center phonon modes has been computed and a new assignment of experimental data has been proposed. The static dielectric tensor has also been obtained; it shows amplitudes comparable to $CaTiO_3$ and is also highly anisotropic. Inspections of the phonon frequencies and of the static dielectric tensor both emphasize that, although from the structural and optical points of view the orthorhombic phase can be considered as a pseudocubic structure, from the dynamical point of view, it is highly anisotropic.

Acknowledgments

This work was supported by the European STREP MaCoMuFi, the Volkswagen Stiftung and the European Network of Excellence FAME-EMMI. The simulations have been performed on the supercomputer MareNostrum at the Barcelona Supercomputing Center—Centro Nacional de Supercomputacion (The Spanish National Supercomputing Center).

References

[1] Martin C, Maignan A, Hervieu M and Raveau B 1999 *Phys. Rev.* B **60** 12191
[2] Loshkareva N N, Nomerovannya L V, Mostovshchikova E V, Makhnev A A, Sukhorukov Yu P, Solin N I, Arbuzova T I, Naumov S V, Kostromitina N V, Balbashov A M and Rybina L N 2004 *Phys. Rev.* B **70** 224406
[3] Wollan E O and Koehler W C 1955 *Phys. Rev.* **100** 545
[4] Poeppelmeir K R, Leonowicz M E, Scanlon J C, Longo J M and Yelon Y B 1982 *J. Solid State Chem.* **45** 71
[5] Matar S F 2003 *Prog. Solid State Chem.* **31** 239
[6] Jung J H, Kim K H, Eom D J, Noh T W, Choi E J, Yu J, Kwon Y S and Chung Y 1997 *Phys. Rev.* B **55** 15489
[7] Freyria Fava F, Arco Ph D', Orlando R and Dovesi R 1997 *J. Phys.: Condens. Matter* **9** 489
[8] Nicastro M and Patterson C H 2002 *Phys. Rev.* B **65** 205111
[9] Gonze X, Beuken J-M, Caracas R, Detraux F, Fuchs M, Rignanese G-M, Sindic L, Verstraete M, Zerah G, Jollet F, Torrent M, Roy A, Mikami M, Ghosez Ph, Raty J-Y and Allan D C 2002 *Comput. Mater. Sci.* **25** 478–92
[10] Hartwigsen C, Goedecker S and Hutter J 1998 *Phys. Rev.* B **58** 3641
[11] Gonze X and Lee C 1997 *Phys. Rev.* B **55** 10355
[12] Taguchi H, Nagao M, Sato T and Shimada M 1989 *J. Solid State Chem.* **78** 312
[13] Rabe K M and Ghosez Ph 2007 *Top. Appl. Phys.* **105** 117
[14] Jung J H *et al* 1997 *Phys. Rev.* B **55** 15489
[15] Abrashev M V *et al* 2002 *Phys. Rev.* B **65** 184301
[16] Cockayne E and Burton B P 2000 *Phys. Rev.* B **62** 3735
[17] Ghosez Ph, Michenaud J-P and Gonze X 1998 *Phys. Rev.* B **58** 6224
[18] Ghosez Ph, Gonze X and Godby R W 1997 *Phys. Rev.* B **56** 12811
[19] Filippetti A and Hill N A 2002 *Phys. Rev.* B **65** 195120
[20] Perebeinos V and Allen P B 2001 *Phys. Rev.* B **64** 085118
[21] Fedorov I, Lorenzana J, Dore P, De Marzi G, Maselli P, Calvani P, Cheong S W, Koval S and Migoni R 1999 *Phys. Rev.* B **60** 11875